IETA International Information and Engineering Technology Association

International Journal of Heat and Technology

Vol. 43, No. 5, October, 2025, pp. 1734-1748

Journal homepage: http://iieta.org/journals/ijht

Thermodynamic Modeling and Energy Efficiency Optimization of Energy Systems in Tourist Attractions



Bingna Lou^{1*}, Sheng Zhao², Yanjie Du³

- ¹ Management Department, Shijiazhuang College of Applied Technology, Shijiazhuang 050800, China
- ² Education Training and Appraisal Center, Hebei Urban and Rural Construction School, Shijiazhuang 050031, China
- ³ Engineering Department, Hebei Province Village and Town Construction Promotion Center, Shijiazhuang 050051, China

Corresponding Author Email: 2004110267@sjzpt.edu.cn

Copyright: ©2025 The authors. This article is published by IIETA and is licensed under the CC BY 4.0 license (http://creativecommons.org/licenses/by/4.0/).

https://doi.org/10.18280/ijht.430512

Received: 27 February 2025 Revised: 9 July 2025 Accepted: 29 July 2025

Available online: 31 October 2025

Keywords:

tourist attractions, integrated energy system, thermodynamic modeling, exergy efficiency, multi-objective optimization, NSGA-III algorithm, energy efficiency optimization, low-carbon transition

ABSTRACT

Under the dual context of the "dual carbon" goals and the pursuit of high-quality tourism development, energy systems in tourist attractions face core challenges, including severe load fluctuations, mismatched energy grades, and difficulties in achieving low-carbon and high-efficiency coordination. To achieve a coordinated optimization of economic, environmental, and energy efficiency objectives, a systematic study was conducted. First, multi-scale system boundaries were defined, and the coupling characteristics among electrical, thermal, and cooling loads with visitor behavior, seasonal rhythms, and weather variations were analyzed from temporal and spatial dimensions. The hierarchical criteria for high- and low-grade energy demands were established, and an integrated energy system architecture featuring "renewable energy as the primary source and fossil energy as a backup" was designed. Second, based on the first and second laws of thermodynamics. detailed thermodynamic models of key components such as photovoltaic (PV) systems, wind turbines, and heat pumps were developed. Through the coupling of energy and material flows, a system-level steady-state and dynamic simulation model was constructed, enabling precise characterization of energy conversion processes and exergy losses. Finally, considering the multi-objective conflict, nonlinearity, and high dimensionality inherent in the optimization problem, an improved Non-dominated Sorting Genetic Algorithm III (NSGA-III) algorithm was proposed to construct a multi-objective optimization model with the goals of minimizing total operating cost and carbon emissions while maximizing system exergy efficiency. The optimal operational strategy was obtained under constraints such as energy balance and equipment operating limits. The main innovations of this study include (a) establishing a "spatiotemporal coupling and energygrade stratification" framework for analyzing load characteristics in tourist attractions, (b) constructing a full-chain thermodynamic model incorporating exergy efficiency, and (c) proposing an improved NSGA-III algorithm adapted to the multi-variable coupling characteristics of tourist attractions. The results demonstrate that the proposed model and algorithm significantly enhance the overall performance of tourist attraction energy systems, providing theoretical and technical support for the planning, design, and operational optimization of integrated energy systems in such environments. This research holds substantial engineering application value for promoting the green and low-carbon transformation of the tourism industry.

1. INTRODUCTION

Driven by the global "dual carbon" goals [1, 2] and the pursuit of high-quality tourism development [3, 4], tourist attractions—characterized as high-energy-consuming, multisectoral composite service systems—have reached a critical juncture in transforming their energy consumption structures and enhancing energy efficiency, both of which are essential for sustainable development [5]. In recent years, the tourism industry in China has continued to expand, resulting in a rigid increase in energy demand within tourist attractions [6]. However, traditional energy systems generally suffer from issues such as a single energy supply structure, delayed load

response, and mismatched energy grades [7, 8]. During peak tourist seasons, heavy reliance on fossil fuels to meet high loads has led to surges in carbon emissions, whereas in off-peak periods, low-load operation has caused difficulties in the utilization of renewable energy. Moreover, the direct use of high-grade electrical energy to meet low-grade thermal and cooling demands has resulted in severe exergy losses. These contradictions not only increase the operational costs of tourist attractions but also impede their transition toward green and low-carbon development [9]. At the same time, energy loads in tourist attractions exhibit pronounced spatiotemporal nonuniformity, as they are strongly influenced by visitor activity patterns, seasonal variations, and weather conditions

[10]. When combined with the stochastic output characteristics of renewable energy sources such as PV and wind power, the operational complexity of the energy system is further intensified, posing significant challenges to conventional planning and optimization methodologies [11].

Extensive research has been conducted domestically and internationally to address the optimization of integrated energy systems. Regarding load characteristic analysis, most existing studies have focused on scenarios such as industrial parks and urban communities [12-14], emphasizing macroscopic statistical descriptions of load features. However, insufficient attention has been paid to the unique operational characteristics of tourist attractions, which exhibit intense fluctuations in service-oriented loads and the coexistence of multi-grade energy demands. Fine-grained analyses that elucidate the coupling mechanisms between thermal/cooling loads and visitor behavior remain lacking. In terms of thermodynamic modeling, many studies have relied solely on the first law of thermodynamics to construct energy balance models [15-17], neglecting the quantification of exergy losses arising from differences in energy grades. Consequently, such models fail to accurately reflect the intrinsic nature of system energy efficiency. Regarding optimization algorithms, traditional multi-objective optimization methods [18-26] often suffer from imbalanced convergence and distribution when addressing high-dimensional objectives. Furthermore, these algorithms have not been adapted to accommodate the coupled characteristics of discrete on/off variables and continuous output variables that are prevalent in tourist attractions, thereby limiting the engineering feasibility of their optimization results. Overall, existing research has yet to establish a comprehensive technical framework tailored to the operational characteristics of tourist attractions that integrates thermodynamic fundamentals with advanced optimization algorithms. As a result, current approaches remain insufficient to meet the practical demands of achieving low-carbon, highefficiency, and economically coordinated optimization in tourist attraction energy systems.

To address the aforementioned research gap, a systematic study was conducted on the integrated energy systems of tourist attractions, following the core logical framework of characteristic analysis-thermodynamic modeling-multiobjective optimization. First, multi-scale system boundaries were defined, and the fluctuation patterns of electrical, thermal, and cooling loads were analyzed from spatiotemporal dimensions. High- and low-grade energy demands were distinguished to establish a foundation for subsequent modeling and optimization. Second, based on the first and second laws of thermodynamics, a refined model of key components-such as PV panels, wind turbines, and heat pumps—was developed. By coupling energy and material flows, a system-level steady-state and dynamic simulation model was constructed, enabling precise depiction of energy conversion processes and exergy losses. Finally, considering the multi-objective conflict, nonlinearity, and high dimensionality inherent in the optimization problem of tourist attractions, an improved NSGA-III algorithm was selected and three-dimensional modified. Α objective encompassing economic, environmental, and efficiency objectives was formulated, and global optimization of system operation strategies was achieved under constraints such as energy balance and equipment operating limits.

The innovations of this study are reflected in three main aspects: (a) A spatiotemporal coupling and energy-grade

stratification framework for load characteristic analysis in tourist attractions was proposed, quantifying the coupling mechanisms among visitor behavior, seasonal rhythms, and energy demand, while establishing energy-grade matching criteria for various service types. (b) A full-chain thermodynamic model incorporating exergy efficiency was constructed, overcoming the limitations of conventional energy balance models and achieving a dual characterization of both the quantity and quality of energy. (c) A load-coupling-based population initialization and hierarchical constraint-handling strategy was introduced to improve the NSGA-III algorithm, enabling adaptation to the multi-variable coupling characteristics of tourist attractions and enhancing convergence and engineering feasibility in high-dimensional optimization problems.

The research outcomes are expected to provide theoretical and technical support for the planning, design, and operational optimization of integrated energy systems in tourist attractions. These results possess significant engineering application value in promoting the transformation of energy consumption structures, reducing carbon emissions, and improving operational efficiency within tourist attractions. The structure of the study is as follows: Section 2 presents the characteristic analysis and thermodynamic modeling of the tourist attraction energy system; Section 3 constructs the multi-objective optimization model and applies the improved algorithm for solution; the subsequent sections validate the effectiveness of the proposed model and algorithm through case studies and provide optimization strategies and recommendations.

2. CHARACTERISTIC ANALYSIS OF ENERGY SYSTEMS IN TOURIST ATTRACTIONS

2.1 Definition of system boundaries

The scientific definition of system boundaries serves as a prerequisite for the thermodynamic modeling and energy efficiency optimization of energy systems in tourist attractions. The core objective lies in clarifying the physical scope, functional boundaries, and temporal dimensions of the study to prevent modeling distortion or deviation of optimization objectives from actual operational requirements caused by ambiguous boundaries. From the physical boundary perspective, the research scope can be divided into three hierarchical levels according to the management structure, spatial distribution, and energy flow characteristics of the tourist attraction: the overall attraction boundary, the functional cluster boundary, and the equipment unit boundary. The overall attraction boundary is defined based on the administrative or natural geographical limits of the attraction. It encompasses all energy-consuming units and energysupplying facilities within the area and is suitable for overall energy planning and macro-level energy efficiency assessment. The functional cluster boundary focuses on subsystems with relatively independent energy consumption characteristics, such as independent resort zones, hotel clusters, and core scenic areas. Within this boundary, the input-output relationships of energy flows are more explicit, facilitating subsystem-level modeling and localized optimization. The equipment unit boundary centers on individual energy-supply or energy-use devices, supporting detailed thermodynamic characterization and optimization of operating parameters at the equipment level.

The functional boundary focuses on the essential structure and interactions of energy flows. It is necessary to identify the types of energy involved, the energy conversion processes, and the relationships among energy flows while excluding auxiliary systems that are not directly connected to the core energy network. This approach ensures that modeling complexity remains manageable. The temporal boundary must correspond to the fluctuation cycles of the attraction's energy load. Typically, an annual timescale is adopted to capture variations across peak and off-peak seasons, while a daily interval is used as the smallest standard time unit to reflect diurnal load fluctuations. For scenarios exhibiting strong short-term volatility, the time resolution can be further refined to the hourly or even minute level to ensure that the model accurately captures the operational characteristics of the energy system across multiple temporal scales.

During boundary definition, adherence to the principles of completeness, independence, and operability is required. Completeness demands that the boundaries include the entire energy chain—from energy supply and distribution to consumption—to ensure comprehensive energy balance analysis. Independence requires that the interactions between the system and its external environment be quantifiable, thus minimizing the influence of uncontrollable factors on modeling precision. Operability ensures that boundary demarcation aligns with the technical feasibility of data acquisition and model computation, maintaining an appropriate balance between research depth and practical engineering applicability.

2.2 Load characteristic analysis

The core characteristics of energy loads in tourist attractions are defined by their service-oriented, open, and seasonal operational attributes, which collectively lead to pronounced spatiotemporal nonuniformity. Moreover, different energy-use types exhibit distinct patterns of load fluctuation and energy-grade demand, which serve as fundamental references for the architectural design and thermodynamic optimization of integrated energy systems in tourist attractions.

From the temporal dimension, load fluctuations display a multi-scale superposition feature, primarily driven by four factors: seasonal variation, diurnal rhythm, holiday effects, and weather disturbances. At the seasonal scale, alternating peak and off-peak tourist seasons induce significant annual periodic fluctuations in energy demand. During peak seasons, the number of visitors typically reaches three to five times that of the off-season, leading to synchronous increases in airconditioning cooling loads, heating loads, hotel hot water demand, and power consumption from recreational facilities. The peak cooling load in the summer high season can reach four to six times that of the off-season, while the peak heating load in the winter season is approximately 2.5 to 3 times higher. In contrast, off-season periods are characterized by a sharp decline in visitor numbers, with energy consumption dominated by essential operational loads. The overall load intensity during these periods is only one-fifth to one-third of that observed in peak seasons. At the diurnal scale, load fluctuations are strongly coupled with the rhythm of visitor activities. Daytime hours correspond to the load peak period, encompassing high-frequency energy-use scenarios such as amusement facility operation, restaurant services, and scenic transportation. During this period, electrical, cooling, and thermal loads rise concurrently. Nighttime loads are primarily associated with hotel accommodation energy use, with intensity reduced to one-third to one-half of the daytime peak, reaching the lowest levels between 1:00 a.m. and 4:00 a.m.

The holiday effect and sudden surges in visitor flow further intensify short-term load volatility. During extended holidays such as the National Day and Spring Festival, the daily peak load can reach two to three times that of regular working days, with significantly prolonged peak durations. Extreme weather conditions also alter load characteristics by influencing visitor behavior and energy demand. For instance, under high-temperature conditions, air-conditioning cooling loads increase by approximately 30%–50% compared with normal weather, whereas heavy rainfall causes a sharp decline in outdoor amusement facility loads and a slight rise in indoor restaurant and retail facility loads.

Corresponding to the multi-scale temporal fluctuations, the spatial nonuniformity of load distribution originates from differences in energy-use attributes across functional zones within the tourist attraction. The hotel cluster area constitutes the primary energy consumption unit, accounting for approximately 40%-60% of the total heating load and 30%-45% of the cooling load, with relatively stable load intensity. The amusement facility area is dominated by power loads, representing 20%–30% of the total electrical load, and exhibits significant short-term fluctuations. The transportation system load is mainly concentrated along primary traffic corridors where electric vehicle charging stations are distributed, showing a "point-distributed, time-concentrated" pattern; during peak hours, charging loads account for 15%-25% of the total electrical demand. In contrast, public and landscape lighting loads are distributed along roads, plazas, and scenic corridors, exhibiting a "linear-planar combined" spatial pattern, with load peaks occurring exclusively at night. In addition, the coupling between different regional loads is relatively weak. For example, the peak heating load in the hotel area and the peak electrical load in the amusement area occur at different times. This temporal offset creates favorable conditions for multi-energy complementarity and peak load shifting.

2.3 Analysis of energy-grade demand analysis

According to the second law of thermodynamics, the energy demand in tourist attractions can be categorized into high- and low-grade energy demands, distinguished based on the minimum driving energy grade required by the energy-consuming equipment. The difference between these two categories directly determines the selection of the energy supply system and the pathway for cascade utilization of energy.

High-grade energy is primarily represented by electricity, whose exergy value approaches 100%. It is mainly utilized to meet demands involving mechanical drive, precision control, and high-quality lighting. Typical application scenarios include electric motor drives for amusement facilities, power supply for electric vehicle charging stations, operation of elevators and ventilation equipment, precision airconditioning control in hotels and office areas, and Light Emitting Diode (LED) lighting systems. The defining characteristics of such high-grade energy demands are their requirement for high energy conversion efficiency, rapid response, and irreplaceability by low-grade energy without incurring significant exergy losses. High-grade energy

demand in tourist attractions accounts for approximately 45%–60% of total energy consumption, with fluctuations strongly correlated to the intensity of visitor activities. During peak tourist seasons, the maximum demand can reach three to four times that observed in the off-season.

Low-grade energy primarily includes medium- and lowtemperature thermal energy as well as medium- and hightemperature cooling energy, both characterized by relatively low exergy values. These forms of energy are mainly consumed to meet comfort-oriented energy demands. The domestic hot water load represents the most significant lowgrade thermal load, with a stable temperature requirement ranging between 45°C and 55°C. This demand is concentrated in hotel guestrooms, restaurant kitchens, and public bathing facilities, with peak loads occurring synchronously with guest washing and dining periods. The space heating load, typically within a temperature range of 20°C to 26°C, is concentrated in the winter peak season and is strongly influenced by the geographical location of the tourist attraction. In northern regions, the heating period generally lasts 3-6 months, with a load intensity of 80-120 W/m², whereas in southern regions, heating demand occurs only during short cold spells. The airconditioning cooling load, with a temperature range of 7°C to 12°C, constitutes the core load during the summer peak season. Its load intensity ranges between 100-150 W/m² and is jointly influenced by outdoor temperature, solar radiation, and visitor density. Low-grade energy demand accounts for approximately 40%-55% of the total energy consumption. Its fluctuation is primarily driven by seasonal variation, climatic conditions, and accommodation occupancy rates, with a relatively smoother temporal distribution compared to highgrade energy demand.

It is noteworthy that a significant issue of energy-grade mismatch exists in tourist attractions. A considerable portion of low-grade energy demands continues to rely on the direct supply of high-grade electrical energy, resulting in reduced overall energy utilization efficiency. Simultaneously, the temporal mismatch between the generation characteristics of distributed renewable high-grade electricity and the actual load profiles further exacerbates energy waste. Therefore, the explicit identification and classification of energy-grade demands constitute a critical prerequisite for achieving cascade energy utilization and enhancing the exergy efficiency of integrated energy systems in tourist attractions.

2.4 Design of the energy system architecture

Based on the spatiotemporal nonuniformity and differentiated energy-grade characteristics of energy loads in tourist attractions, the architectural design of integrated energy systems should adhere to the principles of multi-energy complementarity, cascade utilization, flexible regulation, and low-carbon efficiency. A full-chain coordinated system encompassing the energy supply side, distribution side, consumption side, and energy storage side should be established to effectively address load fluctuations, enhance renewable energy utilization, and reduce system exergy losses.

Figure 1 illustrates the schematic architecture of the integrated energy system for tourist attractions. On the energy supply side, a configuration pattern of "renewable energy as the primary source, fossil energy as the backup, and multi-energy synergistic complementarity" is adopted. The core objective is to optimize the capacity ratios and operational strategies of different supply units according to the attraction's

resource endowment and load characteristics. The supply units of the renewable energy supply serve as the central components. PV systems are prioritized for installation on hotel rooftops, parking canopies, and the roofs of scenic buildings, thereby utilizing idle spaces through distributed access modes to meet nearby energy demands and reduce transmission losses. Wind power systems are suitable for attractions with abundant wind resources, with site selection requiring careful consideration of ecological protection constraints. The ground-source heat pump system, leveraging the stable temperature of soil or groundwater, functions as the core supply unit for low-grade cooling and heating loads. It can meet approximately 60%-80% of the total heating and airconditioning cooling demand, with a coefficient of performance (COP) ranging between 3 and 6, significantly higher than that of conventional systems.

In addition, the solar thermal collector system operates synergistically with the ground-source heat pump, primarily serving domestic hot water needs and capable of covering approximately 50%-70% of the total hot water load. The fossil energy supply subsystem acts as a backup and reliability assurance mechanism. Gas-fired boilers are operated during winter heating peaks, extreme low-temperature events, or periods of renewable energy shortage to supplement thermal demand gaps. Diesel generators are reserved exclusively for emergency scenarios such as grid failures, ensuring the reliability of power supply to critical energy-consuming units. The grid-interactive unit provides essential flexibility regulation for the system. It compensates for renewable energy shortfalls and facilitates the export of surplus electricity generated by distributed sources within the attraction. Through time-of-use electricity pricing mechanisms, the unit guides the system toward optimal operation while reducing overall operating costs.

The energy consumption side architecture is designed with the core principle of "zonal division, energy-grade differentiation, and demand-oriented supply," optimizing the configuration of energy-use equipment and supply modes according to the specific characteristics of each functional area. For the hotel cluster, which represents the primary energy consumption zone, a configuration of "central air-conditioning system + domestic hot water circulation system + distributed lighting system" is adopted. The central air-conditioning system operates synergistically with the ground-source heat pump and solar thermal collector system. The domestic hot water system employs a dual-backup configuration of "solar thermal collector + electric auxiliary heating." The lighting system utilizes LED energy-saving fixtures equipped with intelligent sensing control modules. In the amusement facility area, where power load dominates, a configuration of "dedicated charging piles + electric drive systems" is implemented. The layout and charging strategy of charging piles are optimized according to operational schedules and power demand profiles. Independent PV power systems are deployed for outdoor amusement facilities to supply lighting and emergency power, thereby reducing dependence on the central grid. The transportation system of the tourist attraction is primarily composed of electric shuttle vehicles, supported by a distributed charging network. The layout is efficiently integrated with main transport corridors, visitor transfer hubs, and hotel entrances. A "slow-charging-dominant, fastcharging-supplementary" model is applied to accommodate diverse charging requirements under different operational scenarios. For public service areas, such as restaurants and

shopping centers, decentralized air-conditioning and local ventilation systems are adopted, with operational parameters dynamically adjusted in response to real-time occupant density. Public and landscape lighting systems are equipped with intelligent control systems that automatically regulate brightness and operating schedules according to natural light intensity and visitor flow, effectively reducing unnecessary energy consumption.

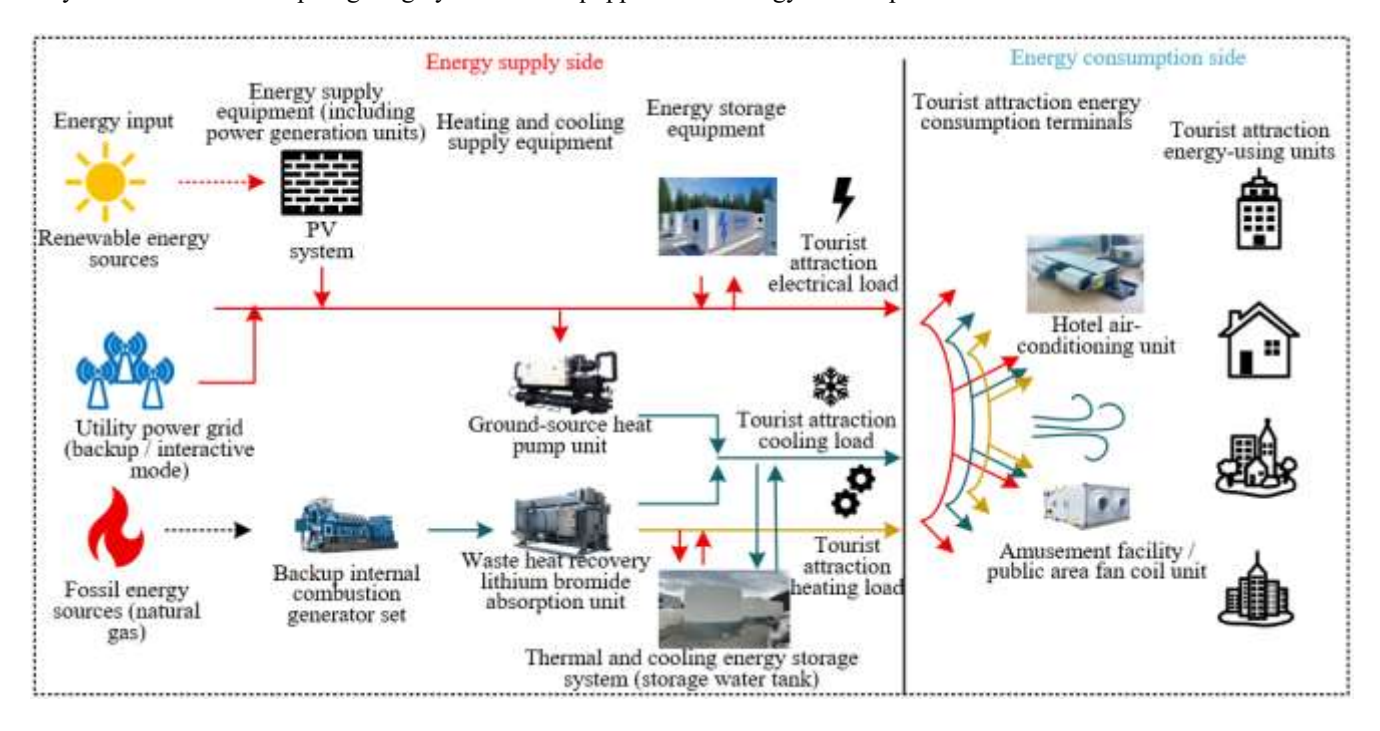


Figure 1. Schematic architecture of the integrated energy system for tourist attractions

The energy storage side constitutes a key subsystem for mitigating spatiotemporal load imbalances, employing a multi-dimensional configuration of electrical, thermal, and cooling energy storage. The electrical energy storage units are sized based on the installed capacities of PV and wind power systems as well as the peak-to-valley load difference. These units primarily serve to smooth renewable generation fluctuations, perform peak shaving and valley filling, and provide emergency backup power. The thermal energy storage system operates in coordination with solar thermal collectors and ground-source heat pumps, storing excess thermal energy during low-demand periods and releasing it during hot water demand peaks. The cooling energy storage system produces and stores ice using off-peak electricity at night, supplying cooling during daytime air-conditioning peaks, thereby reducing grid pressure and operational costs. The energy transmission and distribution side is designed with the goals of "short distance, low loss, and high reliability." The layout of pipelines and electrical lines is optimized. Cooling and heating pipelines are constructed with high-performance insulation materials, and routing is planned to minimize transmission distances. Electrical distribution lines are predominantly installed underground to preserve the scenic integrity of the attraction while optimizing cable cross-sections to reduce transmission losses. The transmission and distribution system is equipped with intelligent monitoring and control modules for real-time supervision of pipeline pressure, temperature, current, and voltage. Faults or leaks can thus be promptly detected, ensuring safe and efficient system operation.

3. THERMODYNAMIC MODELING OF THE ENERGY SYSTEM IN TOURIST ATTRACTIONS

Based on the preceding analysis of the physical boundaries,

load characteristics, and system architecture of energy systems in tourist attractions, the thermodynamic modeling was established on the fundamental principles of the law of energy conservation and the law of entropy increase. A hierarchical modeling framework was adopted, combining componentlevel refined modeling with system-level coupled modeling, to construct a mathematical model capable of accurately representing the mechanisms of energy conversion, transfer, and dissipation within the system. The developed model is required to comprehensively account for the spatiotemporal fluctuations of energy loads, the stochastic nature of renewable energy outputs, and the multi-energy complementary characteristics of the system. This provides a robust quantitative analytical tool for energy efficiency optimization and operational strategy formulation in subsequent research and practical applications. Several key assumptions were established during the modeling process: (a) The effect of pressure loss in the transmission and distribution network on energy grade is neglected, and only temperature-induced exergy losses are considered. (b) All components are assumed to operate under quasi-steady-state conditions, where dynamic responses are simplified as steady-state superpositions within each time step. (c) During the charging and discharging processes of energy storage devices, parameters such as temperature and pressure are assumed to be uniformly distributed, thereby avoiding the additional complexity caused by local thermodynamic nonequilibrium.

3.1 Component-level thermodynamic model

The component-level model serves as the foundation of the entire system model. It was established for the key equipment within the tourist attraction energy system—including PV modules, wind turbines, heat pumps, energy storage units, and boilers—to quantify the relationships between their input—

output characteristics and critical operating parameters. Moreover, exergy analysis indicators were incorporated to evaluate and quantify energy utilization efficiency, ensuring the thermodynamic consistency of the overall modeling framework.

3.1.1 PV system model

The core function of the PV system is to convert solar irradiance into electrical energy, with its output characteristics primarily influenced by solar radiation intensity, ambient temperature, and the aging condition of the PV modules. Based on the law of energy conservation, the output power model of the PV system can be expressed as:

$$P_{pv}(t) = P_{stc} \cdot \frac{G(t)}{G_{stc}} \cdot \left[1 + k\left(T_c(t) - T_{stc}\right)\right] \cdot \eta_{pv} \tag{1}$$

The temperature model of the PV cell is given by:

$$T_c(t) = T_a(t) + \frac{NOCT - 20}{800} \cdot G(t)$$
 (2)

where, $P_{pv}(t)$ denotes the PV output power at time t (kW); P_{stc} represents the rated output power under standard test conditions (STC) (kW); G(t) is the total solar irradiance at time t (W/m²); G_{stc} is the standard irradiance under STC, equal to 1000 W/m²; $T_c(t)$ denotes the PV cell temperature (°C); $T_a(t)$ represents the ambient temperature (°C); T_{stc} is the standard cell temperature, set at 25°C; k is the power temperature coefficient, equal to -0.0045/°C; η_{pv} denotes the combined efficiency of the inverter and electrical wiring, typically ranging between 0.92 and 0.96; and NOCT is the nominal operating cell temperature, ranging from 45°C to 48°C.

3.1.2 Wind power generation system model

In tourist attractions, small-scale distributed wind turbines are predominantly employed, and their output power exhibits a nonlinear dependence on wind speed. To accurately describe this relationship, the power characteristic model was developed based on the law of energy conservation, incorporating the operational constraints of cut-in, rated, and cut-out wind speeds. The output power of the wind turbine can be expressed as:

$$P_{wt}(t) = \begin{cases} 0, v(t) \le v_{ci} \text{ or } v(t) \ge v_{co} \\ \frac{1}{2} \rho A v(t)^{3} C_{p} \eta_{wt}, v_{ci} < v(t) < v_{r} \\ P_{rated}, v_{r} < v(t) < v_{co} \end{cases}$$
(3)

where, $P_{wt}(t)$ denotes the wind turbine output power at time t (kW); v(t) represents the wind speed at hub height (m/s); v_{ct} is the cut-in wind speed, typically between 3–4 m/s; v_{co} is the cut-out wind speed, typically 25 m/s; v_r is the rated wind speed, generally between 12–15 m/s; ρ represents the air density, equal to 1.225 kg/m³; A denotes the swept area of the wind turbine rotor (m²); C_p is the power coefficient, typically ranging from 0.35 to 0.45; η_{wt} represents the generator efficiency, within 0.90–0.95; and P_{rated} denotes the rated power output of the turbine (kW).

3.1.3 Heat pump system model

The heat pump system serves as the core component for

supplying low-grade heating and cooling loads in tourist attractions. Its performance is directly influenced by the evaporation temperature and condensation temperature. Based on the first law of thermodynamics, the performance model under heating and cooling conditions was formulated below. The heating COP is expressed as:

$$COP_{h}(t) = \eta_{carnot} \cdot \frac{T_{cond}(t)}{T_{cond}(t) - T_{evan}(t)}$$
(4)

The cooling COP is expressed as:

$$COP_{c}(t) = \eta_{carnot} \cdot \frac{T_{evap}(t)}{T_{cond}(t) - T_{evap}(t)}$$
(5)

The power balance relationship of the heat pump system is given by:

$$P_{hp}(t) = \frac{Q_{heating}(t)}{COP_h(t)} = \frac{Q_{cooling}(t)}{COP_c(t)}$$
(6)

where, $COP_h(t)$ represents the heating COP; $COP_c(t)$ denotes the cooling COP; $T_{cond}(t)$ and $T_{evap}(t)$ are the condensation and evaporation temperatures, respectively (K); η_{carnot} is the Carnot efficiency factor, typically ranging from 0.5 to 0.7; $P_{hp}(t)$ denotes the input electrical power of the heat pump (kW); and $Q_{heating}(t)$ and $Q_{cooling}(t)$ represent the heating power and cooling power, respectively (kW).

3.1.4 Energy storage system models

The energy storage system in tourist attractions encompasses electrical, thermal, and cooling storage subsystems. Separate charge–discharge characteristic models were established for each, with emphasis placed on efficiency degradation, self-discharge, and state constraints. The electrical energy storage model was developed based on the law of energy conservation, describing the relationship between charging/discharging power and the state of charge (SOC), while incorporating charge–discharge efficiency and self-discharge rate corrections. The expression is formulated as:

$$\frac{dSOC_{bat}(t)}{dt} = \frac{\eta_{ch}P_{ch}(t) - \frac{P_{dis}(t)}{\eta_{dis}}}{E_{bat}^{max}}$$
(7)

The thermal energy storage model accounts for both latent and sensible heat storage in phase change materials, establishing the relationship between temperature and stored thermal energy under energy conservation principles:

$$\frac{dSOC_{tes}(t)}{dt} = \frac{Q_{ch}(t) - Q_{dis}(t)}{E_{tes}^{max}} \cdot \eta_{tes}$$
 (8)

The cooling energy storage model utilizes the latent heat of ice melting to store cold energy. Its mathematical formulation is analogous to that of the thermal energy storage model, with the principal difference lying in the exergy computation of cold energy and the phase change parameters. The phase change temperature was set at 0°C, and the latent heat of the

phase change was taken as 334 kJ/kg. The operational constraints corresponding to the aforementioned models are expressed as:

$$\begin{cases} SOC_{\min} \leq SOC(t) \leq SOC_{\max} \\ 0 \leq P_{ch}(t) \leq P_{ch}^{\max} \\ 0 \leq P_{dis}(t) \leq P_{dis}^{\max} \\ P_{ch}(t) \cdot P_{dis}(t) = 0 \end{cases}$$

$$(9)$$

where, SOC(t) denotes the state of charge, ranging from 0 to 1; η_{ch} and η_{dis} represent the charging and discharging efficiencies, respectively, typically within 0.92–0.98; $P_{ch}(t)$ and $P_{dis}(t)$ denote the charging power and discharging power (kW); E^{max}_{bat} is the maximum capacity of the battery storage system (kWh); E^{max}_{tes} represents the maximum capacity of the thermal storage tank (kWh); η_{tes} denotes the thermal storage efficiency, generally ranging between 0.85 and 0.95; and δ_{sd} refers to the self-discharge rate (%/day).

3.1.5 Gas boiler model

The gas boiler functions as a backup heat source in tourist attractions, with its primary purpose being the conversion of the chemical energy of natural gas into thermal energy. Based on the first law of thermodynamics, the energy balance equation for the boiler system is established as follows:

$$Q_{boiler}(t) = \eta_{boiler} \cdot \dot{m}_{fuel}(t) \cdot LHV_{fuel}$$
(10)

The exergy efficiency of the boiler is calculated according to the following expression:

$$\eta_{ex,boiler} = \frac{\dot{E}x_{out}}{\dot{E}x_{in}} = \frac{\dot{Q}\left(1 - \frac{T_0}{T_{steam}}\right)}{\dot{m}_{fuel} \cdot ex_{fuel}}$$
(11)

where, $Q_{boiler}(t)$ denotes the boiler thermal output power (kW); η_{boiler} represents the boiler thermal efficiency, typically ranging from 0.85 to 0.95; $\dot{m}_{fuel}(t)$ is the mass flow rate of the fuel (kg/s); LHV_{fuel} denotes the lower heating value of the fuel (kJ/kg); $\eta_{ex,boiler}$ represents the exergy efficiency of the boiler; T_{steam} is the steam temperature (K); T_0 denotes the ambient temperature (K); and ex_{fuel} represents the specific exergy of the fuel (kJ/kg).

3.2 System-level coupling model

At the system level, the aforementioned component models were coupled through energy flow, mass flow, and information flow, thereby forming a comprehensive thermodynamic model that encompasses the entire "energy supply—transmission and distribution—consumption—storage" chain. The system-level model is classified into steady-state and dynamic categories, corresponding respectively to the planning and design and operational optimization phases of the energy system in tourist attractions.

(a) Steady-state model

The system energy balance equations were formulated based on the law of energy conservation, with their primary objective being the matching between total energy supply and total energy demand, while ensuring that the operational constraints of all components are satisfied. Taking a typical day under steady operating conditions in a tourist attraction as an example, the system energy balance equations are expressed below. The electricity balance, thermal energy balance, cooling energy balance, and exergy balance equations, respectively, are expressed as follows:

$$P_{grid}(t) + P_{pv}(t) + P_{wt}(t) + P_{dis}^{bat}(t)$$

$$= P_{load}^{elec}(t) + P_{ch}^{bat}(t) + P_{hr}(t) + P_{other}(t)$$
(12)

$$Q_{boiler}(t) + COP_h(t) \cdot P_{hp}(t) + Q_{dis}^{tes}(t)$$

$$= H_{load}(t) + Q_{ch}^{tes}(t) + H_{loss}(t)$$
(13)

$$COP_{c}(t) \cdot P_{bn}(t) + Q_{dis}^{tes}(t) = C_{load}(t) + Q_{ch}^{ces}(t) + C_{loss}(t)$$
 (14)

$$\sum \dot{E}x_{in} = \sum \dot{E}x_{out} + \sum \dot{E}x_{destruction} + \sum \dot{E}x_{loss}$$
 (15)

where, $P_{grid}(t)$ denotes the purchased power from the utility grid (kW); $P^{elec}_{load}(t)$ represents the electrical load (kW); $H_{load}(t)$ denotes the thermal load (kW); $C_{load}(t)$ represents the cooling load (kW); $H_{loss}(t)$ and $C_{loos}(t)$ indicate the heat network loss and cooling network loss (kW), respectively; Ex represents the exergy flow rate (kW); and $Ex_{destruction}$ denotes the exergy destruction rate (kW). The system energy performance indicators include energy utilization efficiency and exergy efficiency, defined as follows:

$$EUF = \frac{\sum (Useful\ Output\ Energy)}{\sum (Input\ Primary\ Energy)}$$
(16)

$$\eta_{ex,system} = \frac{\sum (Output \ Exergy)}{\sum (Input \ Exergy)}$$
 (17)

(b) Dynamic model

To account for the intra-day fluctuations in load demand and the short-term variability of renewable energy output, a dynamic simulation model was developed using a time-step method. The core of this model lies in incorporating the dynamic response characteristics of components into the steady-state framework. For example, the dynamic temperature response model of PV modules, which is influenced by thermal inertia, can be expressed as $T=T+(G\cdot\alpha$ - $U \cdot (T-T) \cdot \Delta t / (m \cdot c)$, where α is the absorption coefficient of the PV module, U denotes the overall heat loss coefficient, mrepresents the mass of the PV module, and c is the specific heat capacity of the module. The dynamic model outputs include the time-dependent operational parameters of each component, the system-level energy performance indicators, and the interactive power. These simulations were typically implemented using professional platforms MATLAB/Simulink or TRNSYS.

4. ENERGY EFFICIENCY OPTIMIZATION OF THE TOURIST ATTRACTION ENERGY SYSTEM

4.1 Optimization problem and objective function

The energy efficiency optimization of the integrated energy

system in tourist attractions fundamentally aims to achieve synergistic enhancement of system performance under a complex, multi-energy coupled environment, characterized by source-load randomness and multiple interacting constraints. This process is accomplished through the dynamic regulation of decision variables. The core of this optimization framework lies in constructing a comprehensive modeling system that integrates problem definition, variable representation, objective coupling, and constraint quantification. The optimization design presented in this section focuses on defining the essential elements of the problem, taking into account the operational characteristics of tourist attractions, such as significant fluctuations in service-oriented loads, a high proportion of renewable energy, and a strong demand for multi-energy complementarity. Within this framework, the optimization boundaries and decision variable dimensions were explicitly defined. A multi-objective function system was developed to encompass the key performance dimensions of economic efficiency, environmental sustainability, and energy performance. Moreover, the coupling mechanisms and trade-off logic among these objectives were systematically elaborated, providing a theoretical foundation for subsequent application of advanced optimization algorithms.

4.1.1 Definition of the optimization problem and representation of decision variables

The scientific definition of the optimization problem must be grounded in the precise alignment between system boundaries and operational scenarios. Based on the thermodynamic model developed in Section 2, the optimization boundary is defined to encompass the entire "energy supply-storage-transmission and distribution-consumption" chain. The temporal scale extends across annual, daily, and hourly levels, while the spatial scale corresponds to the full spatial extent of the tourist attraction, covering functional subregions such as hotel clusters, recreational facilities, and public service areas. Representative operating scenarios were established for various typical conditions—peak-season weekdays, peak-season holidays, off-season weekdays, and extreme weather events—to ensure the general applicability of the model.

The selection of decision variables must simultaneously satisfy the principles of control feasibility and state completeness, allowing for a comprehensive representation of both the operational states and regulatory actions within the system. These decision variables are categorized into continuous variables and binary variables according to their characteristics. The continuous variables include $P_{grid}(t)$, which is the purchased power from the grid at time t (kW); $P_{sell}(t)$, which is the power sold to the grid at time t (kW); $P_{boiler}(t)$, which is the thermal output of the gas boiler (kW); $P_{hp,h}(t)$, which is the heating power of the heat pump (kW); $P_{hv,c}(t)$, which is the cooling power of the heat pump (kW); $P_{chbat}(t)$, which is the charging power of the battery (kW); $P_{dishat}(t)$, which is the discharging power of the battery (kW); $Q_{chtes}(t)$, which is the charging thermal power of the thermal storage tank (kW); $Q_{distes}(t)$, which is the discharging thermal power of the thermal storage tank (kW); $SOC_{bat}(t)$, which is the SOC of the battery (0-1); and $SOC_{tes}(t)$, which is the SOC of the thermal storage tank (0-1). The binary variables include $u_{boiler}(t)$, which is the on/off state of the gas boiler (0/1); $u_{hp}(t)$, which is the on/off state of the heat pump (0/1); $u_{chbat}(t)$, which is the charging state of the battery (0/1); and $u_{disbat}(t)$, which is the discharging state of the battery (0/1).

All decision variables must conform to the principle of physical feasibility, ensuring that their values are consistent with equipment operational mechanisms, tourist attraction management rules, and external regulatory constraints. This principle establishes the foundation for the formulation of subsequent constraint conditions.

4.1.2 Construction of the multi-objective function and coupling mechanism

The core objective of optimizing the energy system of a tourist attraction is to achieve synergistic coordination among economic controllability, environmental sustainability, and energy efficiency enhancement. These three goals correspond respectively to the economic, environmental, and energy performance dimensions of the system. Due to their inherent coupling and trade-offs, a multi-objective optimization function must be established, wherein weighting coefficients are employed to quantify the relative priority of each objective, reflecting the operational orientation of the tourist attraction.

(a) Economic objective: minimization of total operating cost

Economic performance constitutes the fundamental constraint of system operation in tourist attractions. The total operating cost (C) includes the fuel consumption cost, grid interaction cost, equipment operation and maintenance (O&M) cost, and start-up/shutdown cost. This total cost must be accurately quantified based on the system composition and operational characteristics of the integrated energy system, as expressed by:

$$\min F_1 = C_{grid} + C_{fuel} + C_{om} - R_{sell}$$
 (18)

Each cost component must be formulated to reflect realistic operational conditions, with specific sub-models derived below. The grid purchasing cost, fuel consumption cost, O&M cost, and electricity selling revenue, respectively, can be expressed as follows:

$$C_{grid} = \sum_{t=1}^{T} \left[c_{buy}(t) \cdot P_{grid}(t) \cdot \Delta t \right]$$
 (19)

$$C_{fuel} = \sum_{t=1}^{T} \left[c_{fuel}(t) \cdot \frac{P_{boiler}(t)}{\eta_{boiler}} \cdot \Delta t \right]$$
 (20)

$$C_{om} = \sum_{t=1}^{T} \left[c_{om,pv} \cdot P_{pv}(t) + c_{om,wt} \cdot P_{wt}(t) + c_{om,hp} \cdot \left(P_{hp,h}(t) + P_{hp,c}(t) \right) + c_{om,boiler} \cdot P_{boiler}(t) \right] \cdot \Delta t$$

$$(21)$$

$$R_{sell} = \sum_{t=1}^{T} \left[c_{sell}(t) \cdot P_{sell}(t) \cdot \Delta t \right]$$
 (22)

(b) Environmental objective: minimization of carbon emissions

In alignment with the national dual-carbon goals and the green development objectives of tourist attractions, the total carbon emissions (E) of the system primarily originate from fossil fuel combustion and electricity purchased from the grid. In contrast, renewable energy systems and energy storage units are assumed to operate with zero direct carbon emissions. Consequently, the optimization objective focuses on increasing the renewable energy utilization rate, reducing fossil fuel consumption, and minimizing dependence on high-

carbon grid electricity. The carbon emission calculation model was formulated based on the Life Cycle Assessment (LCA) approach, considering only the operational phase emissions. The general expression of the model is formulated as follows:

$$\min F_2 = CE_{grid} + CE_{fuel} \tag{23}$$

The specific expressions for each emission source are detailed below. The grid electricity emissions and fuel combustion emissions can be expressed as follows:

$$CE_{grid} = \sum_{t=1}^{T} \left[e_{buy}(t) \cdot P_{grid}(t) \cdot \Delta t \right]$$
 (24)

$$CE_{fuel} = \sum_{t=1}^{T} \left[e_{fuel}(t) \cdot \frac{P_{boiler}(t)}{\eta_{boiler}} \cdot \Delta t \right]$$
 (25)

(c) Energy efficiency objective: maximization of system exergy efficiency

Based on the second law of thermodynamics, exergy efficiency serves as a more accurate indicator of the quality-based utilization efficiency of energy, overcoming the limitation of conventional energy efficiency measures that focus solely on quantity while neglecting energy grade matching. This metric is particularly suited to the multi-grade energy demand and multi-source energy supply coupling characteristics typical of tourist attraction energy systems. The total system exergy efficiency is defined as the ratio between the total useful exergy output on the demand side and the total exergy input on the supply side. The corresponding objective function is expressed as:

$$\max F_{3} = \eta_{ex,system} = \frac{\sum_{t=1}^{T} E_{out}(t)}{\sum_{t=1}^{T} E_{in}(t)}$$
 (26)

The detailed exergy efficiency calculation is given below. The exergy output and input can be expressed as follows:

$$E_{out}(t) = E_{load}^{elec}(t) + E_{load}^{heat}(t) \cdot \left(1 - \frac{T_0}{T_{heat}}\right) + E_{load}^{cool}(t) \cdot \left(\frac{T_0}{T_{cool}} - 1\right)$$
(27)

$$E_{in}(t) = E_{grid}(t) + E_{fuel}(t) + E_{ren}(t)$$
(28)

All parameters are defined as follows: $c_{buy}(t)$ and $c_{sell}(t)$: time-of-use electricity purchase and selling prices (Yuan/kWh); c_{fuel} : unit fuel cost (Yuan/kg or Yuan/m³); $c_{om,*}$: O&M coefficients of each device (Yuan/kWh); Δt : time interval (1 hour); $e_{grid}(t)$ and e_{fuel} : grid and fuel carbon emission factors (kg CO₂/kWh and kg CO₂/kg, respectively); $P^{min/max}_{boiler}$ and $P^{min/max}_{hp}$: minimum/maximum output powers of the boiler and heat pump (kW); E^{max}_{bat} and E^{max}_{tes} : maximum capacities of the battery and thermal storage tank (kWh); $\eta^{bat}_{ch/dis}$: battery charge/discharge efficiency (0.92–0.98); $\eta^{tes}_{ch/dis}$: thermal storage charge/discharge efficiency (0.85–0.95); $P^{elec}_{load}(t)$: the electrical load curve, which includes hotel, lighting, and transportation loads; $H_{load}(t)$: the thermal load curve, including hot water and heating loads; $C_{load}(t)$: the cooling load curve, reflecting air-conditioning and

refrigeration demands; and $P_{other}(t)$: other electrical loads, such as those arising from entertainment facilities.

5. MULTI-OBJECTIVE OPTIMIZATION AND SOLUTION IMPLEMENTATION

The optimization problem constructed for the tourist attraction energy system exhibits pronounced characteristics of multi-objective conflict, nonlinearity, high dimensionality, and strong constraint coupling. Traditional linear optimization methods are inadequate for addressing the coupling of nonlinear and discrete variables, while low-dimensional multiobjective algorithms struggle to balance convergence and distribution performance in high-dimensional scenarios. To overcome these limitations, NSGA-III was adopted as the core algorithm. This section systematically elaborates on the algorithm selection rationale, scenario-specific adaptation strategies, end-to-end solution implementation, performance verification, thereby establishing a closed-loop framework integrating problem formulation, algorithmic logic, and solution realization.

5.1 Algorithm selection: Adaptability analysis of NSGA-III

The selection of the algorithm is guided by four principal criteria: objective dimensional adaptability, variable type constraint-handling compatibility. capability. computational efficiency for engineering applications. Through a comparative analysis of mainstream multiobjective intelligent optimization algorithms, NSGA-III was identified as uniquely suited to the optimization requirements of the tourist attraction energy system. Its adaptability is primarily reflected in three aspects. The first is the highdimensional objective balancing mechanism. NSGA-III introduces a reference-point-based approach that transforms a multi-objective conflict into an association optimization between solutions and a set of uniformly distributed reference points. This design effectively mitigates the core deficiency of NSGA-II, wherein excessive non-dominated solutions under three or more objectives lead to ineffective selection. The second is the compatibility with hybrid variable types. A hybrid encoding strategy combining real-coded representation for continuous variables and binary-coded representation for discrete variables was employed. This dual-variable encoding, coupled with targeted genetic operators, enables precise adaptation to the system's dual control requirementscontinuous power regulation and discrete state switching. The third is the engineering constraint friendliness. NSGA-III incorporates a hierarchical constraint-handling mechanism, allowing direct correspondence to the system's hard energy balance constraints and soft SOC constraints for real engineering scenarios. This approach prevents overconstraining, which may lead to feasible domain shrinkage, as well as constraint relaxation, which could otherwise yield infeasible solutions.

5.2 Adaptation and improvement of NSGA-III for tourist attraction scenarios

To address the inherent limitations of the original NSGA-III when applied to tourist attraction energy systems—namely, the low proportion of feasible solutions in the initial population, weak coupling between fitness evaluation and

optimization objectives, and constraint-handling operations that may induce convergence deviation—targeted adaptations were implemented across three dimensions: population initialization, fitness evaluation, and constraint handling. In terms of population initialization, instead of adopting conventional random initialization, a "typical scenario clustering + pre-constraint verification" strategy was developed. Historical load data from the tourist attraction were first clustered using the K-means algorithm, identifying three representative operating scenarios: peak, off-peak, and valley. For each scenario, key variable initial values were predefined based on scenario features and corresponding population proportions were allocated. Subsequently, all randomly generated individuals underwent pre-verification of device on/off status-output coupling constraints, and infeasible solutions were eliminated before the population was replenished to the preset scale. This approach significantly enhanced both the initial population quality and overall computational efficiency.

In terms of fitness evaluation, to ensure seamless integration between the optimization objectives and the algorithmic evaluation process, a normalized multi-objective function was directly employed as the fitness function. The Analytic Hierarchy Process-Entropy Weight Method (AHP-EWM) was applied to determine the combined weights of each objective, simultaneously accommodating operational preferences of the tourist attraction and objective data-driven information entropy corrections, thereby minimizing bias in weight determination. Furthermore, a clear correspondence was established between the fitness value and the comprehensive performance of each solution, providing explicit optimization direction during algorithmic iteration. To prevent the influence of weight fluctuations on the optimization results, sensitivity analysis was subsequently conducted to verify the robustness of the obtained solutions, ensuring the algorithm's adaptability to variations in weight assignments.

A hierarchical constraint-handling strategy combining "feasible-solution prioritization for hard constraints" and "dynamic penalty functions for soft constraints" was introduced. For hard constraints—including energy balance, device on/off-output coupling, and mutual exclusivity constraints—any violation automatically classifies the individual as a dominated solution, which is forcibly eliminated from the population. This ensures strict adherence to engineering feasibility. For soft constraints, such as SOC upper and lower limits, renewable energy utilization rate, and equipment output boundaries, dynamic penalty coefficients were designed. During early iterations, smaller penalty coefficients were used to encourage broader exploration of the feasible domain; as iterations progressed, penalty coefficients were gradually increased to drive convergence toward feasible regions. This mechanism prevented convergence stagnation due to excessive penalization while avoiding engineering infeasibility resulting from overly relaxed constraints.

5.3 Full-process solution implementation and parameter calibration

The full-process solution implementation follows the logical sequence of "data preprocessing – population initialization – genetic operations – non-dominated sorting – elite preservation – iteration termination." Initially, equipment parameters, load profiles, meteorological data, and economic—

environmental parameters of the tourist attraction were imported. Data cleaning and normalization were conducted to ensure high-quality input for the solution. Following this, the improved population initialization strategy was applied to generate a hybrid-encoded initial population. Simulated binary crossover and single-point crossover were employed for continuous and discrete variables, respectively, while polynomial and bit-flip mutations were adopted to maintain population diversity during evolution. Subsequently, parent and offspring populations were merged, and a hierarchical non-dominated sorting procedure was executed. Elite preservation was achieved through reference point association and crowding distance calculation, ensuring both solution convergence and distribution uniformity. The iterative process terminated when either the maximum number of iterations was reached or the fluctuation of fitness values satisfied the precision criterion, at which point the Pareto-optimal solution set was output.

Parameter calibration is a critical process for ensuring the performance of the algorithm. To this end, four core parameters—population size, crossover probability, mutation probability, and number of iterations—were optimized using an orthogonal experimental design. Multiple parameter combinations were tested, with convergence and distribution metrics (specifically, the spread metric, SP) adopted as evaluation criteria. Through comprehensive simulation-based testing, the optimal parameter combination was determined. Special attention was given to the interaction effects among parameters on the performance of the algorithm, ensuring that parameter combinations improve convergence efficiency without compromising the diversity or distribution quality of solutions. This establishes a highly efficient and stable computational foundation for the optimization of the tourist attraction energy system.

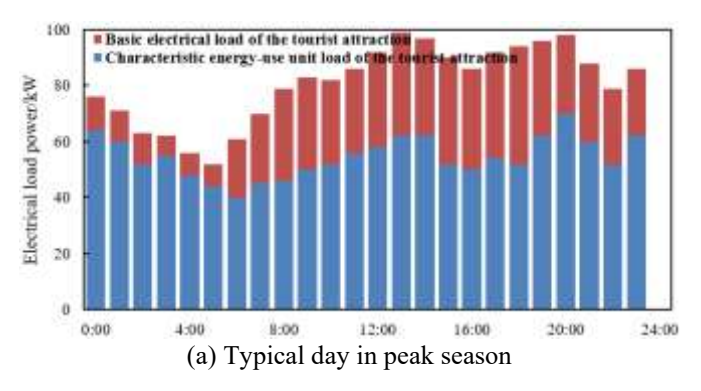
6. EXPERIMENTAL RESULTS AND ANALYSIS

To accurately quantify the spatiotemporal heterogeneity of electrical loads in the tourist attraction and to support subsequent energy system modeling and optimization, an hourly power composition analysis was conducted for typical days during both the peak and off-seasons. The results indicate that, as shown in Figure 2(a), the electrical load during the typical peak-season day exhibits a pronounced daytime highload pattern, with total power remaining above 80 kW between 12:00 and 20:00. During this period, characteristic energy consumption units-including amusement facilities and electric vehicle charging stations—account for over 40% of the total load. This pattern demonstrates a strong correlation with the concentrated daytime activity rhythm of visitors. In contrast, as depicted in Figure 2(b), the overall load level during the typical off-season day declines significantly. The total power during the same high-demand period (12:00-20:00) ranges between 60 and 80 kW, while the share of characteristic energy consumption units drops to below 30%. This reduction directly reflects the suppressed energy demand resulting from the substantial decrease in visitor volume. In summary, the electrical load of the tourist attraction displays distinct spatiotemporal non-uniformity characteristics, characterized by strong seasonal differentiation, pronounced peak-to-valley day-night variation, temporal and concentration of characteristic energy consumption activities.

To accurately characterize the spatiotemporal coupling

characteristics between the electrical load and renewable energy output of the tourist attraction—thereby supporting source—load matching analysis and energy efficiency optimization strategies within the thermodynamic modeling framework—an hourly power analysis of the electrical load, distributed PV output, and distributed wind power generation was conducted for typical days during the peak and off-seasons. The results indicate that, as shown in Figure 3(a), the electrical load during the typical peak-season day exhibits a pronounced daytime high-load pattern, with power remaining consistently above 80 kW between 12:00 and 20:00. The distributed PV output exceeds 60 kW between 8:00 and 16:00, partially overlapping with the load peak period. The distributed wind power output remains relatively stable,

fluctuating between 20 and 40 kW. In contrast, during the typical off-season day shown in Figure 3(b), the overall load level decreases significantly, with power during the high-demand period (12:00–20:00) ranging between 60 and 80 kW. The PV output peak declines to approximately 40 kW, and its active generation window becomes shorter. Simultaneously, the wind power output exhibits smaller fluctuations. In summary, the spatiotemporal coupling between electrical load and renewable energy output in the tourist attraction is characterized by the following pattern: during the peak season, both the load level and PV–load matching degree are high, while during the off-season, both the load demand and renewable generation remain at comparatively low levels.



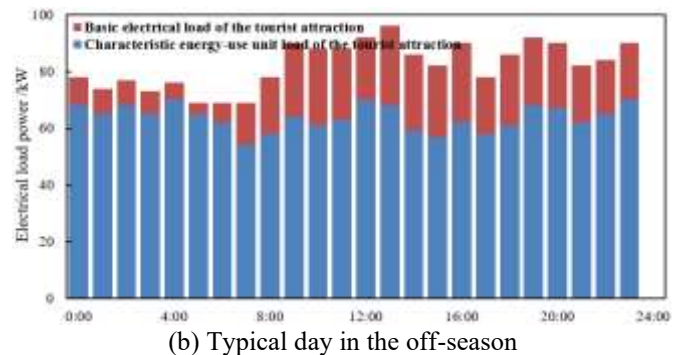
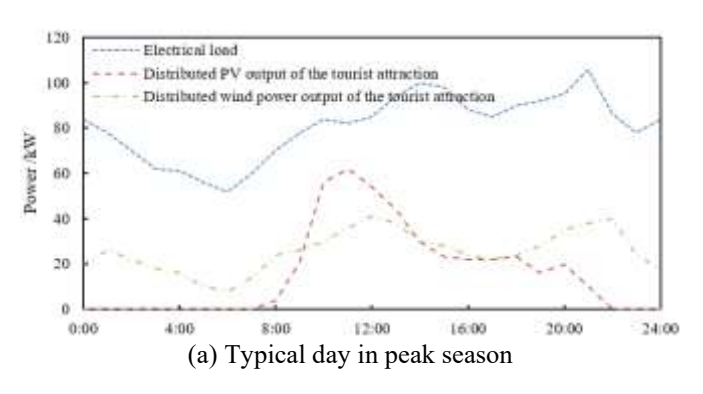


Figure 2. Hourly power composition of electric load in the tourist attraction on typical days (peak season vs. off-season)



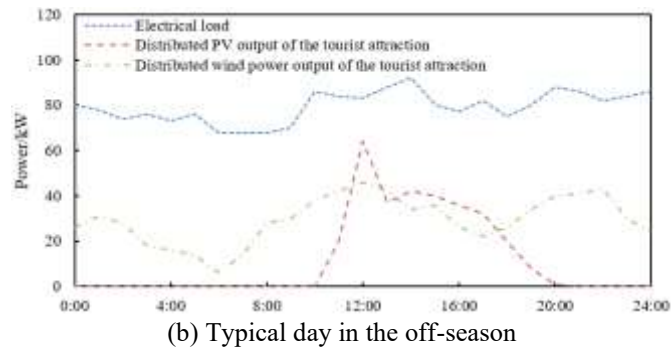
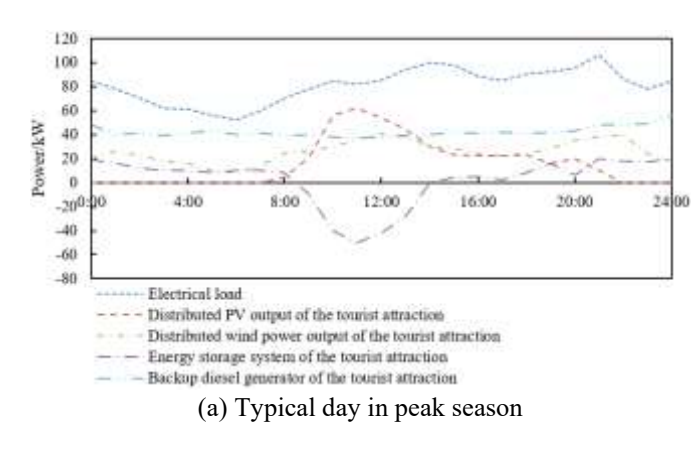


Figure 3. Hourly power variation of electric load and renewable energy output in the tourist attraction (peak season vs. off-season)



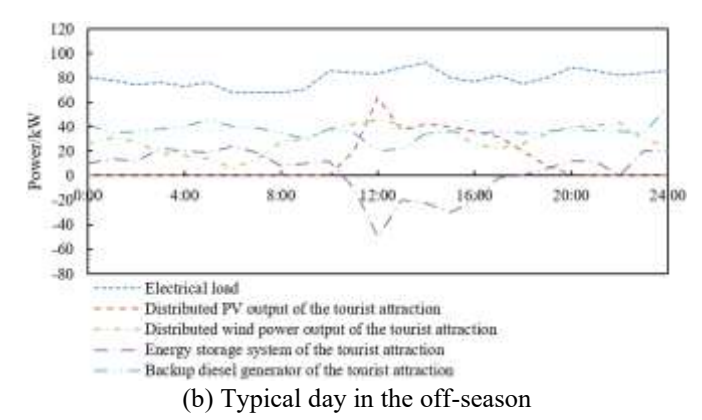


Figure 4. Output curves of each unit in the integrated energy system of the tourist attraction on typical days (peak season vs. off-season)

To quantitatively characterize the dynamic coupling relationships among the electrical load, renewable energy output, energy storage system, and backup power source within the integrated energy system of the tourist attraction and to support source—load matching analysis and the design of multi-unit coordination strategies for energy efficiency

within the thermodynamic optimization modeling framework—an hourly power analysis was conducted for typical days during both the peak and off-seasons. The analysis encompassed electric load, distributed PV output, distributed wind power output, energy storage system operation, and backup diesel generator output. The results indicate that, during the typical peak-season day shown in Figure 4(a), the electrical load exhibits a pronounced daytime peak, while the distributed PV output exceeds 60 kW between 8:00 and 16:00, showing partial temporal coupling with the high-load period. The energy storage system operates in a charging mode during load troughs and discharges stored energy during high-demand periods, effectively achieving peak shaving and valley filling. The backup diesel generator is only marginally activated under short-duration conditions when PV output is insufficient and energy storage discharge is constrained. In contrast, as illustrated in Figure 4(b), during the typical off-season day, the overall electrical load level decreases markedly. The PV output peak contracts to approximately 40 kW, with a shorter active generation period, while the amplitude of charging and discharging in the energy storage system simultaneously diminishes. The diesel generator's operational frequency and intensity also decline significantly. In summary, the output characteristics of each subsystem within the integrated energy system display distinct seasonal differentiation. During the peak season, the electrical load and PV generation exhibit strong coupling, accompanied by a high demand for energy storage regulation, whereas during the off-season, the outputs of all subsystems remain generally subdued, and the system regulation pressure is correspondingly lower.

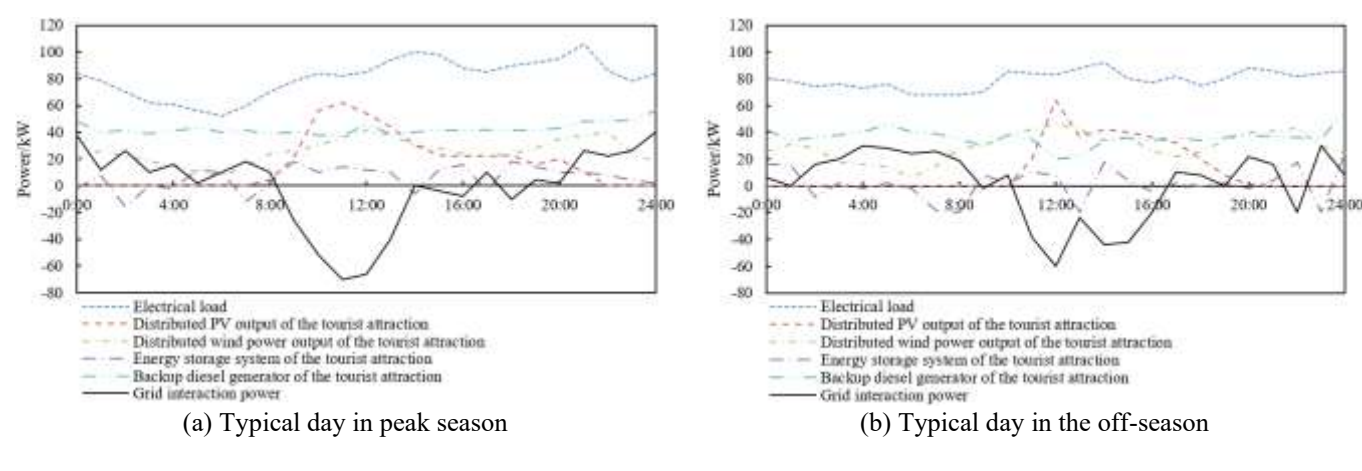


Figure 5. Output curves of each unit in the grid-connected integrated energy system of the tourist attraction (peak season vs. off-season)

To accurately quantify the dynamic coupling characteristics among the electrical load, renewable energy output, energy storage system, backup power source, and grid power interaction within the grid-connected integrated energy system of the tourist attraction—and to support source—load—grid—storage matching analysis and the design of multi-unit coordination strategies for energy efficiency optimization within the thermodynamic modeling framework—an hourly power analysis was performed for typical days during both the peak and off-seasons. This analysis encompassed the electrical load, distributed PV generation, distributed wind power output, energy storage operation, backup diesel generator performance, and grid interaction power.

The results indicate that, during the typical peak-season day shown in Figure 5(a), the electrical load displays a pronounced daytime peak, with power continuously exceeding 80 kW between 12:00 and 20:00. The distributed PV generation provides more than 60 kW from 8:00 to 16:00, exhibiting partial temporal coupling with the high-load period. The energy storage system operates in charging mode during offpeak hours and discharges during the high-load period, thereby achieving peak shaving and valley filling. The power exchange with the main grid shifts dynamically, acting as electricity import during PV shortages and electricity export when PV generation exceeds demand. The backup diesel generator is only activated under short-duration conditions when a sudden drop in PV output coincides with limited storage discharge capacity. As shown in Figure 5(b), during the typical off-season day, the overall electrical load level declines significantly, with the PV output peak contracting to approximately 40 kW and its duration shortened. Correspondingly, the charge–discharge amplitude of the energy storage system decreases, and both the frequency and magnitude of grid power interactions and diesel generator operation exhibit downward trends. In summary, the grid-connected integrated energy system of the tourist attraction demonstrates clear seasonal differentiation in its operational characteristics. During the peak season, strong coupling between electrical load and PV generation necessitates intensive storage and grid regulation, while during the off-season, all subsystems operate at relatively low levels, resulting in reduced system regulation pressure.

To verify the accuracy of the thermodynamic component models and ensure the reliability of system-level modeling, a comparative analysis was performed between the modelpredicted and measured values for key components, including the PV system, ground source heat pump, and energy storage system. As shown in Table 1, the RMSE values for all component models remain below 2.35, and the relative errors are confined within 4.2%. Among them, the electrical energy storage system model demonstrates the highest prediction accuracy, with RMSE = 0.025 and a relative error of 2.5%. The distributed wind turbine model exhibits a slightly higher RMSE, primarily attributed to wind speed measurement uncertainties, yet still falls within engineeringly acceptable These validation results confirm that thermodynamic component models developed in this study can accurately capture the energy conversion and transfer characteristics of each device.

To quantitatively evaluate the trade-offs among economic,

environmental, and energy-efficiency objectives within the multi-objective optimization framework and to provide a decision-making reference for the operation of the tourist attraction, three typical compromise solutions located along the Pareto frontier were analyzed in detail. As shown in Table 2, an increase in economic cost from 1250 Yuan/day to 1520 Yuan/day corresponds to a reduction in carbon emissions from 480 kgCO₂/day to 360 kgCO₂/day, while the exergy efficiency improves from 68.2% to 76.8%. This trend demonstrates a negative correlation between cost and carbon emissions and a positive correlation between cost and exergy efficiency. Simultaneously, the share of PV output increases from 45% to

60%, while both the average charge—discharge power of the energy storage system and the grid interaction power progressively decrease. These variations indicate that solutions with higher exergy efficiency achieve energy performance optimization primarily through enhanced renewable energy utilization and reduced dependence on energy storage and the main grid. Overall, the results confirm that the proposed multi-objective optimization model effectively balances the economic, environmental, and energy-efficiency requirements of the tourist attraction's integrated energy system, thereby providing differentiated decision-making options for operators.

Table 1. Validation results of thermodynamic component model accuracy

Component Type	Model Prediction Range	Measured Range	Root Mean Square	Mean Absolute
Component Type	(kW/kJ)	(kW/kJ)	Error (RMSE)	Error (MAE)
Distributed PV system	0-65	0-62	2.35	1.87
Ground source heat pump (heating)	0-50	0-48	1.92	1.55
Electrical energy storage system	0-100 (SOC)	0-100 (SOC)	0.025	0.020
Distributed wind turbine	0-40	0-38	1.68	1.32
Gas boiler	0-80 (thermal power)	0-78	2.11	1.76

Table 2. Performance indicators of typical compromise solutions in multi-objective optimization

Compromise Solution ID	Economic Cost (Yuan/day)	Carbon Emissions (kgCO ₂ /day)	Exergy Efficiency (%)	PV Output Share (%)	Energy Storage Charging/Discharging State (Average Power, kW)	Grid Interaction Power (Average, kW; Positive for Import)
Solution 1	1250	480	68.2	45	Charge -15 / discharge 20	120
Solution 2	1380	420	72.5	52	Charge -10 / discharge 15	80
Solution 3	1520	360	76.8	60	Charge -5 / discharge 10	40

7. CONCLUSION

This study focused on the integrated energy system of tourist attractions, following a logical framework of analysis-thermodynamic modeling-multicharacteristic objective optimization. Through an analysis of the spatiotemporal coupling patterns between electrical loads, tourist behavior, and seasonal rhythms, it was identified that the energy demand of tourist attractions exhibits strong seasonal differentiation and temporal concentration of characteristic energy use. Based on the first and second laws of thermodynamics, refined models encompassing key components—such as PV generation, heat pumps, and energy storage systems—were established. Experimental validation confirmed that the RMSE values of all component models were below 2.35, with relative errors controlled within 4.2%, thereby achieving accurate characterization of system-level energy conversion and exergy loss. To address the multiobjective conflict inherent in system operation, an improved NSGA-III algorithm was proposed and applied to construct a three-dimensional optimization model integrating economic cost, environmental performance, and energy efficiency. The resulting Pareto frontier solutions demonstrated dynamic trade-offs among cost, carbon emissions, and exergy efficiency, offering differentiated decision-making strategies for the energy management of tourist attractions. The theoretical significance of this study lies in the introduction of a "spatiotemporal coupling and quality grading" load analysis framework combined with a thermodynamic modeling approach incorporating exergy efficiency, which bridges an existing research gap in the fundamental characterization of

energy system behavior and efficiency essence in tourist attractions. The engineering significance is reflected in the proposed improved optimization algorithm and the multi-objective solution set, which provide practical technical support for the planning and operation of integrated energy systems in tourism facilities, thereby contributing to the green and low-carbon transition of the tourism industry.

However, certain limitations remain. First, the model assumptions do not fully capture the dynamic and uncertain nature of real-world operations. Second, the data used were derived from a specific type of tourist attraction, and the general applicability to other tourism formats requires further validation. Future research can be extended in three directions: (a) Enhancement of model refinement, by integrating datadriven dynamic efficiency models and uncertainty prediction methods to improve adaptability to real operational scenarios; (b) Advancement of optimization algorithms, through the incorporation of reinforcement learning to achieve real-time online optimization, enhancing system adaptability to sourceload fluctuations; and (c) Expansion of multi-energy flow coordination, by integrating the coupling of cooling, heating, and electrical loads and comprehensive demand response mechanisms into the optimization framework, to further exploit the energy efficiency improvement potential of integrated energy systems in tourist attractions.

REFERENCES

[1] Li, X., Wu, J., Lin, C. (2025). Decarbonizing provincial construction industry under the "dual carbon" goals: Assessing reduction capacities and charting optimal

- pathways. Building and Environment, 272: 112639. https://doi.org/10.1016/j.buildenv.2025.112639
- [2] Lin, X. (2023). Strategic allocation of building carbon emission rights within urban frameworks: A case study of Henan Province under China's dual carbon objectives. Journal of Urban Development and Management, 2(4): 222-236. https://doi.org/10.56578/judm020405
- [3] Sun, T., Su, J., Zheng, M. (2024). Study on the comprehensive assessment of high-quality development performance of low carbon tourism in China's Rizhao city empowered by new quality productivity. Rocznik Ochrona Środowiska, 26: 493-509. https://doi.org/10.54740/ros.2024.046
- [4] Tandamrong, D., Laphet, J., Gooncokkord, T. (2025). Evaluating carbon credit offsets: Carbon neutral tourism for passengers traveling from Thailand to China. Challenges in Sustainability, 13(4): 535-545. https://doi.org/10.56578/cis130405
- [5] Fotis, P., Korre, M. (2023). The relationship between competition, tourism and sustainable development: Three interdependent topics. Journal of Research, Innovation and Technologies, 2(1): 70-78. https://doi.org/10.57017/jorit.v2.1(3).06
- [6] Soylu, Ö.B., Menegaki, A.N., Bayraktar, Y. (2024). Energy usage trends in top tourist destinations: The role of tourism and trade. Energy Sources, Part B: Economics, Planning, and Policy, 19(1): 2377986. https://doi.org/10.1080/15567249.2024.2377986
- [7] Pavlakovič, B., Demir, M.R., Pozvek, N., Turnšek, M. (2021). Role of tourism in promoting geothermal energy: Public interest and motivation for geothermal energy tourism in Slovenia. Sustainability, 13(18): 10353. https://doi.org/10.3390/su131810353
- [8] Katircioglu, S., Gokmenoglu, K.K., Eren, B.M. (2019). The role of tourism growth in generating additional energy consumption: Empirical evidence from major tourist destinations. Environmental and Ecological Statistics, 26(4): 303-323. https://doi.org/10.1007/s10651-019-00429-0
- [9] Tao, J., Liu, Y., Zhou, C. (2023). Carbon emission measurement and water treatment in Poyang Lake ecoeconomic zone in the context of energy saving and emission reduction in tourism. Desalination and Water Treatment, 299: 222-231. https://doi.org/10.5004/dwt.2023.29680
- [10] Pata, U.K., Balsalobre-Lorente, D. (2022). Exploring the impact of tourism and energy consumption on the load capacity factor in Turkey: A novel dynamic ARDL approach. Environmental Science and Pollution Research, 29(9): 13491-13503. https://doi.org/10.1007/s11356-021-16675-4
- [11] Kuo, N.W., Lin, C.Y., Chen, P.H., Chen, Y.W. (2012). An inventory of the energy use and carbon dioxide emissions from island tourism based on a life cycle assessment approach. Environmental Progress & Sustainable Energy, 31(3): 459-465. https://doi.org/10.1002/ep.10585
- [12] Turdybek, B., Tostado-Véliz, M., Mansouri, S.A., Jordehi, A.R., Jurado, F. (2024). A local electricity market mechanism for flexibility provision in industrial parks involving Heterogenous flexible loads. Applied Energy, 359: 122748. https://doi.org/10.1016/j.apenergy.2024.122748
- [13] Ghamarypour, S., Rahimiyan, M. (2025). Energy

- resources investment for industrial virtual power plants under techno-economic uncertainties. International Journal of Electrical Power & Energy Systems, 164: 110409. https://doi.org/10.1016/j.ijepes.2024.110409
- [14] Alcarruz, C., Mina-Casaran, J.D., Navarro-Espinosa, A. (2022). From passive network to PV urban community microgrids: Finding the optimal size and upgrading cost. Energy for Sustainable Development, 70: 387-402. https://doi.org/10.1016/j.esd.2022.08.005
- [15] Freitas, S., Reinhart, C., Brito, M.C. (2018). Minimizing storage needs for large scale photovoltaics in the urban environment. Solar Energy, 159: 375-389. https://doi.org/10.1016/j.solener.2017.11.011
- [16] Corbari, C., Ravazzani, G., Mancini, M. (2011). A distributed thermodynamic model for energy and mass balance computation: FEST-EWB. Hydrological Processes, 25(9): 1443-1452. https://doi.org/10.1002/hyp.7910
- [17] Wang, Y., Zhu, Q., Huang, T., Han, X., Lin, M. (2024). Modelling and simulation of nonlinear dynamic flow field and temperature field of depyrogenation tunnel. Facta Universitatis, Series: Mechanical Engineering, 22(1): 45-62. https://doi.org/10.22190/FUME221221011W
- [18] Cha, B., Galbraith, S.C., Liu, H., Park, S.Y., et al. (2019). A thermodynamic balance model for liquid film drying kinetics of a tablet film coating and drying process. AAPS Pharmscitech, 20(5): 209. https://doi.org/10.1208/s12249-019-1398-8
- [19] Majewski, D.E., Wirtz, M., Lampe, M., Bardow, A. (2017). Robust multi-objective optimization for sustainable design of distributed energy supply systems. Computers & Chemical Engineering, 102: 26-39. https://doi.org/10.1016/j.compchemeng.2016.11.038
- [20] Alzahrani, A., Hafeez, G., Ali, S., Murawwat, S., Khan, M.I., Rehman, K., Abed, A.M. (2023). Multi-objective energy optimization with load and distributed energy source scheduling in the smart power grid. Sustainability, 15(13): 9970. https://doi.org/10.3390/su15139970
- [21] Mutani, G., Morando, V., Zhou, X., Tayefinasrabad, M., Tundo, A. (2024). An Italian geoportal for renewable energy communities. Journal of Sustainability for Energy, 3(4): 244-264. https://doi.org/10.56578/jse030404
- [22] Wang, Z. (2025). A lightweight AIGC-based multiobjective architectural space generation method: Collaborative optimization of thermal comfort and ventilation performance. International Journal of Heat and Technology, 43(3): 1151-1163. https://doi.org/10.18280/ijht.430332
- [23] Zhang, Q.H., Yuan, R., Hou, Y.J., Feng, Y.K., Wang, J. (2025). Thermodynamic performance analysis and multi-objective optimization design of cooling systems in wind farms. International Journal of Heat and Technology, 43(3): 969-979. https://doi.org/10.18280/ijht.430315
- [24] Hussain, E.S., Suhael, S.M. (2025). Optimization of HVAC Systems: Advances in thermofluid performance modeling and intelligent control strategies. Power Engineering and Engineering Thermophysics, 4(1): 58-85. https://doi.org/10.56578/peet040105
- [25] Qiao, J.F., Niu, Y.J. (2024). Thermodynamic multiobjective optimization: A deep learning and evolutionary algorithm approach. International Journal of Heat and

Technology, 42(4): 1417-1426.

https://doi.org/10.18280/ijht.420431 [26] Man, D.W., Zhang, Y., Tang, L.P., Xu, Q.H., Chen, D., Jiang, B.D., Han, T.T., Xu, T., Li, J.B. (2024). Nonlinear dynamical characteristics of hybrid tri-stable

piezoelectric energy harvester based on rotational motion. Facta Universitatis, Series: Mechanical 257-273. Engineering, 22(2): https://doi.org/10.22190/FUME240118033M